International Journal of Solids and Structures 47 (2010) 730–737

Contents lists available at ScienceDirect

International Journal of Solids and Structures

journal homepage: www.elsevier.com/locate/ijsolstr

The small-scale yielding of shape memory alloys under mode III fracture

S. Desindes [a,*], S. Daly [b]

[a] Ecole Polytechnique, 91120 Palaiseau, France
[b] Department of Mechanical Engineering, University of Michigan, MI 48104, USA

ARTICLE INFO

Article history:
Received 11 August 2009
Received in revised form 27 October 2009
Available online 27 November 2009

Keywords:
Shape memory alloy
Fracture
Constitutive model
Nickel–Titanium
Mode III

ABSTRACT

A model for stress-induced phase transformation surrounding the crack tip during mode III fracture of shape memory alloys (SMAs) is introduced. Considering a state of small-scale yielding and J2 plasticity (loading only), the shape and size of the martensite (M), the austenite (A) and the transformation zone (A → M) are fully determined. For a fixed crack length, the zones of constant strain around the crack tip develop as circles. The width of the A → M transformation zone and the martensite both depend linearly on the crack length. Moreover, the crack tip is surrounded by martensite under plastic deformation. The theoretical model is then extended to examine the mode III fracture behavior of Nickel–Titanium (Nitinol), and these results are compared to FEM analysis of a edge crack torsion (ECT) test for an isotropic material. The size of stress-induced martensite zone in the FEM analysis is underestimated by about 50% from the theoretical model, due largely to the difference in the computed and theoretical stress–strain relation. However, the model and simulation show remarkable agreement on the size of the A → M transformation zone (error<5%), which dominates the region surrounding the crack tip. In addition, the model predictions accurately match the FEM analysis in determining the radii circles of constant strain in the vicinity of the crack tip, and the shape and size of the plastically deformed martensite zone. The results presented in this paper provide a first step to better understand the mechanics of fracture in shape memory alloys under mode III loading.

1. Introduction

Shape memory alloys (SMAs) are metal alloys that exhibit the special characteristics of either large recoverable strains or large induced forces under loads or temperature changes. SMAs have two phases, the high temperature phase called *Austenite* (A), generally B2 cubic, and the low temperature phase called *Martensite* (M) which is tetragonal, monoclinic or orthorhombic. The transformation from one phase to another (A → M or M → A) does not occur by the diffusion of atoms but by shear lattice distortion. One of their most interesting mechanical behaviors is known as the *pseudoelastic effect*. If external stresses are applied slightly above the transformation temperature, SMAs produce large recoverable strains after the linear elastic limit. After unloading, the reverse martensitic transformation occurs and the transformation strain is recovered almost completely. As SMAs (especially Nickel–Titanium) are widely used in fields such as aeronautics and the medical industry, where durability is a crucial issue, it becomes necessary to understand the mechanical response of these materials when cracks are present.

The fracture process of these alloys is closely related to the evolution of local strain and martensitic transformation at the crack tip. Yi and Gao (2000) and Yi et al. (2001) examined the fracture toughening mechanism of shape memory alloys numerically under mixed mode I and II loading due to martensite transformation. They showed that stress-induced martensitic transformation reduces the crack tip energy release rate and increases toughness. There has also been other significant research on the fatigue behavior of Nitinol, stemming mainly from its suitability for medical applications such as stents, guidewires or braided catheters (for example see Duerig et al. (1996) and the references contained therein). Fracture studies have focused on the two plane modes of fracture propagation (I and II), in part because of the ability to observe these modes through experiment. Wang et al. (2005, 2007) investigated the formation of stress-induced martensite in front of cracks under mode I and II loading. They found that the size of martensitic and (A → M) transformation zones increase with crack length, that cracks propagate into the stress-induced martensite, and that the formation of martensite has similarities with results in plasticity. Daly et al. (2007) performed an experimental investigation of mode I crack initiation in thin sheets of Nitinol. They observed the formation of stress-induced martensite near the crack tip and obtained full-field quantitative mappings of the surface strain fields associated with transformation, which indicate that phase transformation contributes to toughening around the crack tip. Robertson et al. (2007) examined the formation of stress-induced martensite in

* Corresponding author. Tel.: +33 6 12 69 48 03.
E-mail address: simon.desindes@polytechnique.edu (S. Desindes).

0020-7683/$ - see front matter © 2009 Elsevier Ltd. All rights reserved.
doi:10.1016/j.ijsolstr.2009.11.014

mode I loading using a synchrotron X-Ray microdiffusion analysis. There are known limitations using isotropic homogeneous yield criteria (e.g. the dimension of the plastic zone found by this method is often overestimated), exposed by Lexcellent and Schloemerkemper (2007). But Robertson et al. (2007) showed that the size and shape of the transformation zone may be considered by drawing comparisons to the plastic zone size, as estimated from linear elastic fracture mechanics (LEFM).

Although there has been substantial work towards understanding the fracture behavior of SMAs under mixed mode I and II (Yi and Gao, 2000; Freed and Banks-Sills, 2007; Gollerthan et al., 2009; Wang et al., 2005, 2007; Daly et al., 2007; Robertson et al., 2007), the equally important issue of fracture under mode III loading has received little attention, in part due to the difficulty of experimental observations (Tschegg, 1982; Qian and Fatemi, 1996; Pokluda and Pippan, 2005; Pokluda et al., 2008). As the use of SMAs necessitates mixed mode loading including mode III, it is necessary to investigate the influence of mode III loading on the fracture toughening mechanism of SMAs.

In this paper, we present a theoretical model for the evolution of stress-induced martensite around the crack tip under mode III loading, and compare it to FEM analysis of a crack edge torsion test for an isotropic SMA. We consider the antiplane case of longitudinal shear involving displacements in the direction perpendicular to the cracked plane. The model is based from J2 plasticity, assuming a volume preserving deformation and pressure-independent material behavior. Thus, it is valid only upon loading. Accurate determination of stress and deformation fields near cracks employing realistic stress–strain relations are of fundamental importance for the mechanical description of fracture and fatigue, but are often accompanied by mathematical difficulties which prevent the determination of an analytical solution. A particular class of problems involving cracks subjected to uniform remotely applied stress fields, allowing considerably simplified expressions for the strain and stress tensors, have an explicit solution. The following analysis is inspired by the work of Rice on fracture calculations under mode III plastic deformation (Rice, 1967, 1968). In order to extend the Rice's analysis to model the fracture behavior of shape memory alloys under loading, the plastic stress–strain relation (Rice, 1967, 1968) is adapted to account for the pseudoelastic effect observed with SMAs. The constitutive model is compared with finite element calculations for the representative SMA Nickel–Titanium.

2. Theory

2.1. Basic equations in strain plane

In this analysis, SMAs are assumed to be elastic and isotropic. Following Rice (1967), we suppose that deformations are small and that a linear relation exists between the principal stress tensor $\underline{\underline{\tau}}$ and the strain tensor $\underline{\underline{\gamma}}$. Thus, the stress–strain relation is specified by a function $\tau = \tau(\gamma)$:

$$\tau = \sqrt{\tau_x^2 + \tau_y^2} \quad \gamma = \sqrt{\gamma_x^2 + \gamma_y^2} \tag{1}$$

where $\tau_x = \tau_{xz}, \tau_y = \tau_{yz}, \gamma_x = \gamma_{xz}, \gamma_y = \gamma_{yz}$.

Considering the speed of deformation to be sufficiently small and neglecting the acceleration and the variation of temperature, the equations of compatibility and equilibrium can be rewritten by introducing a scalar potential function $\psi = \psi(\gamma)$,

$$\underline{\nabla}_\gamma \times \psi = 0 \tag{2}$$

$$\underline{\nabla}_\tau \cdot \psi = 0 \tag{3}$$

$$\text{with} \quad \underline{\nabla}_\gamma = \underline{e}_x \frac{\partial}{\partial \gamma_x} + \underline{e}_y \frac{\partial}{\partial \gamma_y}, \quad \underline{\nabla}_\tau = \underline{e}_x \frac{\partial}{\partial \tau_x} + \underline{e}_y \frac{\partial}{\partial \tau_y}$$

where $\underline{e}_x$ is in the crack direction and $\underline{e}_x$ is perpendicular to the crack (see Fig. 1) Following Rice, substitution into the equilibrium Eq. (3) and use of the strain-stress relations leads to a linear differential equation for ψ. The equation takes its simplest form in polar coordinates in the strain plane (Rice, 1967). Let ϕ be the angle between the y direction and the principal shear direction, measured positive counterclockwise. When the strain potential function is expressed in terms of γ and ϕ, the Cartesian coordinates of a point in the material are given by

$$x = -\sin\phi \frac{\partial \psi}{\partial \gamma} - \frac{\cos\phi}{\gamma} \frac{\partial \psi}{\partial \phi} \tag{4}$$

$$y = \cos\phi \frac{\partial \psi}{\partial \gamma} - \frac{\sin\phi}{\gamma} \frac{\partial \psi}{\partial \phi} \tag{5}$$

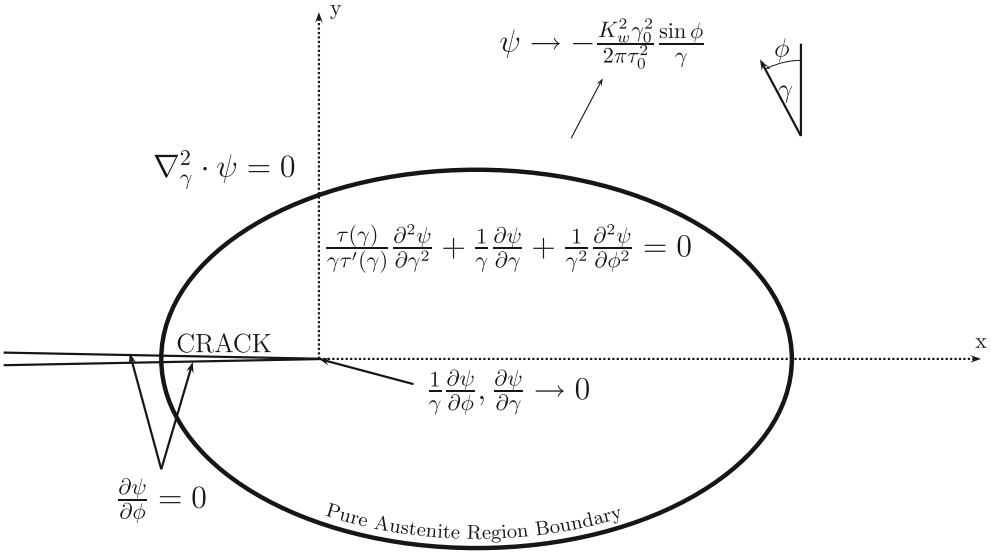

Fig. 1. Formulation of the edge crack problem for a material subjected to antiplane strain.

and the equilibrium Eq. (3) may be written

$$\frac{\tau(\gamma)}{\gamma\tau'(\gamma)}\frac{\partial^2\psi}{\partial\gamma^2}+\frac{1}{\gamma}\frac{\partial\psi}{\partial\gamma}+\frac{1}{\gamma^2}\frac{\partial^2\psi}{\partial\phi^2}=0 \tag{6}$$

where $\tau'(\gamma)=\partial\tau/\partial\gamma$.

If one has a linear elastic material ($\tau(\gamma)=G\gamma$ and therefore $\frac{\tau(\gamma)}{\gamma\tau'(\gamma)}=1$), equilibrium (Eq. (6)) reduces to the Laplace form $\nabla^2_\gamma\cdot\psi=0$.

2.2. Boundary conditions

Fig. 1 represents the problem studied. One considers a crack along the *X*-axis, with a crack tip at *x=y=0*. The material is subjected to an applied remote stress (τ_∞) which respects the equilibrium equation and which induces an antiplane displacement. Since $y=0$ on the crack surfaces, Eqs. (4) and (5) require

$$\frac{\partial\psi}{\partial\phi}=0 \quad \text{at} \quad \phi=\pm\pi/2 \tag{7}$$

There is a strain singularity at the crack tip ($x=y=0$), thus

$$\frac{1}{\gamma}\frac{\partial\psi}{\partial\phi}\to 0 \quad \frac{\partial\psi}{\partial\gamma}\to 0 \quad \gamma\to\infty \tag{8}$$

Following Rice (1967), the requirement of an asymptotic approach to the elastic singularity leads to

$$\psi\to-\frac{K^2_{III}\gamma_0^2}{2\pi\tau_0^2}\frac{\sin\phi}{\gamma} \quad \gamma\to 0 \tag{9}$$

2.3. Power-Law hardening materials

To model the mechanical behavior observed in an SMA, we use the elastic–plastic model shown in Fig. 2. The stress–strain relation used is inspired by the uniaxial material model observed by Wang et al. (2008). The Austenite region has a linear elastic loading behavior when a load is first applied (*Zone I*). As the load increases further to an applied principal stress τ_1, the material reaches *Zone II* corresponding to the interval where the A → M phase transformation takes place. In this model the stress is approximated to be constant in Zone II. Lastly, *Zone III* represents the linear elastic deformation of the martensite, and *Zone IV* indicates when the martensite is subjected to irreversible plastic deformation that will not be recovered upon unloading the material. These zones are mathematically described as follows,

Zone I(Elastic deformation of the Austenite phase) : $\tau(\gamma)=\frac{\tau_1}{\gamma_1}\gamma$ (10)

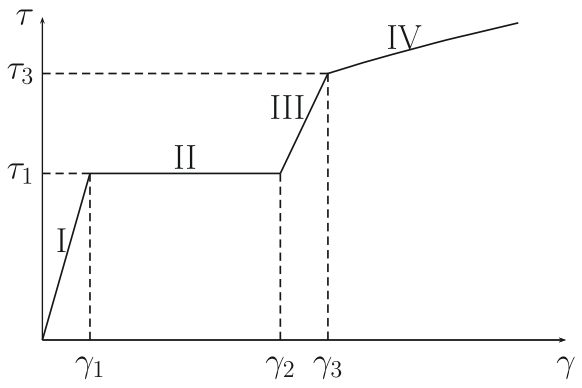

Fig. 2. Model for the mechanical behavior of a shape memory alloy.

Zone II(Phase Transformation A → *M*) : $\tau(\gamma)=\tau_1$ (11)

Zone III(Elastic deformation of the Martensite phase) :

$$\tau(\gamma)=\frac{\tau_3-\tau_1}{\gamma_3-\gamma_2}(\gamma-\gamma_2)+\tau_1 \tag{12}$$

Zone IV(Plastic deformation of the Martensite phase) :

$$\tau(\gamma)=\tau_3\left(\frac{\gamma}{\gamma_3}\right)^n \tag{13}$$

Our model is based on J_2 plasticity and thus only represents the loading path of the SMA. The strain-hardening factor of the martensite (n) present in Eq. (13) may vary between zero and one, where $n=0$ describes perfect plasticity and $n=1$ describes perfect elasticity. In Fig. 2 we choose $n=0.34$ to approximate the behavior of Nickel–Titanium observed by Wang et al. (2008). The yield strain of the Martensite (γ_3) is often quite high, typically around 8%, resulting in a nominally straight line predicted by Eq. (13) and shown in Fig. 2 (Zone IV).

2.4. Small-scale yielding near a crack

We assume that a state of small-scale yielding exists for which the dimensions of the plastic zone are negligible in comparison to notch depth ($r/a<100$, where a is the length of the crack and r the characteristic length of the plastic zone). This assumption is equivalent to

$$s=\frac{\tau_\infty}{\tau_1}\ll 1 \tag{14}$$

Although such small-scale yielding solutions for cracks are mathematically exact only in the limit of a vanishingly small plastic zone, these have been found to be highly accurate approximations to available solutions up to substantial values of s (typically $s<0.5$) (Rice, 1967).

2.5. General solutions

The solutions proposed in this section were obtained by Rice (1967) for a state of small-scale yielding in an elastoplastic material. A brief overview is given here; the reader interested in the mathematical details is invited to read the prior work of Rice (1967) and Muskhelishvili (1953). To respect equilibrium (Eq. (6)) and the boundary conditions (Eqs. (7)–(9)), the potential ψ_i is given by Rice (1967)

$$\psi_i=-\frac{\gamma_1}{\pi\tau_1}K^2_{III}\left[\gamma_{i-1}\int_{\gamma_{i-1}}^{\infty}\frac{du}{u^2\tau(u)}\right]\sin\phi, \quad i=II,III,IV \tag{15}$$

where

$$K_{III}=\tau_\infty\sqrt{\pi a} \tag{16}$$

The physical coordinates corresponding to a given strain in these zones are

$$x=\frac{K^2_{III}}{2\pi\tau_1^2}\left(\frac{\gamma_1\tau_1}{\gamma\tau(\gamma)}\cos 2\phi+\left[2\gamma_1\tau_1\int_\gamma^\infty\frac{du}{u^2\tau(u)}-\frac{\gamma_1\tau_1}{\gamma\tau(\gamma)}\right]\right) \tag{17}$$

$$y=\frac{K^2_{III}}{2\pi\tau_1^2}\frac{\gamma_1\tau_1}{\gamma\tau(\gamma)}\sin 2\phi \tag{18}$$

By direct observation,

$$[x-X(\gamma)]^2+y^2=R(\gamma)^2 \tag{19}$$

is the equation of a circle centered at the distance $X(\gamma)$ ahead of the crack tip and with radius $R(\gamma)$, given by :

$$X(\gamma) = \frac{K_{III}^2}{2\pi\tau_1^2}\left[2\gamma_1\tau_1\int_{\gamma}^{\infty}\frac{du}{u^2\tau(u)} - \frac{\gamma_1\tau_1}{\gamma\tau(\gamma)}\right] \tag{20}$$

$$R(\gamma) = \frac{K_{III}^2}{2\pi\tau_1^2}\frac{\gamma_1\tau_1}{\gamma\tau(\gamma)} \tag{21}$$

Following Rice's elastic solution and considering only a linear elastic loading of austenite (*Zone I*), the potential is

$$\psi_I = -\frac{K_{III}^2\gamma_1^2}{2\pi\tau_1^2}\left(\frac{1}{\gamma} + \frac{\gamma}{\gamma_1^2}\left[2\gamma_1\tau_1\int_{\gamma_1}^{\infty}\frac{du}{u^2\tau(u)} - 1\right]\right)\sin\phi \tag{22}$$

Thus,

$$x = X(\gamma_1) + R(\gamma)\cos 2\phi \tag{23}$$

$$y = R(\gamma)\sin 2\phi \tag{24}$$

In this region, the line of constant strain is a circle, whose center $X(\gamma)$ is independent of $\gamma < \gamma_1$. $R(\gamma_1)$ and $X(\gamma_1)$ both depends on crack length a.

3. Extension to phase transformation: determination of $X(\gamma)$ and $R(\gamma)$ for each zone

To model the pseudoelastic effect of SMAs, we extend the elastoplastic solutions proposed by Rice to Zones II–IV of our material model (Fig. 2), corresponding to all zones where martensite is present. Using the general solutions (Eqs. (17), (18), (23) and (24)) the strain-stress relations presented in Eqs. (10)–(13) are used to determine the zone profiles near the crack tip. The radius, $R(\gamma)$ and the center of a circle of constant strain, $X(\gamma)$ are determined for each zone boundary (i.e. for $\gamma = \gamma_1, \gamma_2, \gamma_3$).

As long as one considers a point in the zone corresponding to the linear elastic loading of the austenite (Zone I), it is straightforward to determine that $X(\gamma)$ stays constant (the center of all circles is $X(\gamma_1)$) whereas $R(\gamma)$ is inversely proportional to γ.

As soon as $\gamma \geqslant \gamma_1$, Eqs. (20) and (21) characterize the center and the radius of the circle. For $\gamma = \gamma_1$, the transformation from $A \to M$ begins,

$$\begin{aligned} X(\gamma_1) &= \frac{K_{III}^2}{2\pi\tau_1^2}\left[2\gamma_1\tau_1\int_{\gamma_1}^{\infty}\frac{du}{u^2\tau(u)} - 1\right] \\ &= \frac{K_{III}^2}{2\pi\tau_1^2}\left[2\gamma_1\tau_1\left\{\frac{(\gamma_3-\gamma_2)^2}{(\tau_1\gamma_3-\tau_3\gamma_2)^2}\left(\frac{\tau_1}{\gamma_2} - \frac{\tau_3}{\gamma_3} + \frac{\tau_3-\tau_1}{\gamma_3-\gamma_2}\ln\frac{\gamma_2\tau_3}{\gamma_3\tau_1}\right)\right.\right. \\ &\quad \left.\left. + \frac{1}{\tau_1}\frac{\gamma_2-\gamma_1}{\gamma_1\gamma_2} + \frac{1}{n+1}\frac{1}{\tau_3\gamma_3}\right\} - 1\right] \end{aligned} \tag{25}$$

$$R(\gamma_1) = \frac{K_{III}^2}{2\pi\tau_1^2} \tag{26}$$

In Zone II ($\gamma_1 \leqslant \gamma \leqslant \gamma_2$), the $A \to M$ phase transformation takes place. Following the same procedure as above, we determine the center and the radius

$$\begin{aligned} X(\gamma) &= X(\gamma_1) - R(\gamma_1)\left[2\tau_1\gamma_1\int_{\gamma_1}^{\gamma}\frac{du}{u^2\tau(u)} - \left(1 - \frac{\gamma_1}{\gamma}\right)\right] \\ &= X(\gamma_1) - \frac{\gamma-\gamma_1}{\gamma}R(\gamma_1) \end{aligned} \tag{27}$$

$$R(\gamma) = \frac{\gamma_1}{\gamma}R(\gamma_1) \tag{28}$$

In Zone III ($\gamma_2 \leqslant \gamma \leqslant \gamma_3$), the phase transformation is macroscopically complete and the martensite is now subject to a linear elastic deformation as the applied load increases. The circles of constant strain are given by

$$\begin{aligned} X(\gamma) &= X(\gamma_2) \\ &\quad + R(\gamma_1)\left[2\tau_1\gamma_1\int_{\gamma}^{\gamma_2}\frac{du}{u^2\tau(u)} + \frac{\gamma_1}{\gamma_2} - \frac{\gamma_1\tau_1}{\gamma\tau(\gamma)}\right] = X(\gamma_2) \\ &\quad + R(\gamma_1)\left[2\tau_1\gamma_1\left\{\frac{(\tau_3-\tau_1)(\gamma_2-\gamma_3)}{(\tau_1\gamma_3-\tau_3\gamma_2)^2}\ln\frac{\gamma\tau_1(\gamma_2-\gamma_3)}{\gamma_2((\tau_1-\tau_3)\gamma-\tau_1\gamma_3+\gamma_2\tau_3)}\right.\right. \\ &\quad \left.\left. + \frac{\gamma_2-\gamma_3}{\tau_1\gamma_3-\tau_3\gamma_2}\frac{\gamma-\gamma_2}{\gamma\gamma_2}\right\} + \frac{\gamma_1}{\gamma_2} - \frac{\gamma_1\tau_1}{\gamma\left[\frac{\tau_3-\tau_1}{\gamma_3-\gamma_2}(\gamma-\gamma_2)+\tau_1\right]}\right] \end{aligned} \tag{29}$$

$$R(\gamma) = R(\gamma_1)\frac{\gamma_1\tau_1}{\gamma\left[\frac{\gamma-\gamma_2}{\gamma_3-\gamma_2}(\tau_3-\tau_1)+\tau_1\right]} \tag{30}$$

where $\gamma = \gamma_3$ defines the elastic–plastic boundary of the martensitic phase, whose center and radius are

$$X(\gamma_3) = \frac{1-n}{1+n}\frac{\tau_1\gamma_1}{\tau_3\gamma_3}R(\gamma_1) \tag{31}$$

$$R(\gamma_3) = \frac{\gamma_1\tau_1}{\gamma_3\tau_3}R(\gamma_1) \tag{32}$$

In Zone IV ($\gamma \geqslant \gamma_3$), the martensite is subject to irreversible deformation. The circle of constant strain in this zone is defined by

$$X(\gamma) = \frac{1-n}{1+n}\frac{\tau_1\gamma_1}{\tau_3\gamma_3}R(\gamma_1)\left[\frac{\gamma_3}{\gamma}\right]^{n+1} \tag{33}$$

$$R(\gamma) = \frac{\tau_1\gamma_1}{\tau_3\gamma_3}R(\gamma_1)\left[\frac{\gamma_3}{\gamma}\right]^{n+1} \tag{34}$$

Clearly the different Zones (I–IV) must not overlap, in order to prevent a zone in the material from existing simultaneously in two different states. The following relations hold for all possible γ_i,

$$\begin{aligned} &X(\gamma_2) + R(\gamma_2) < X(\gamma_1) + R(\gamma_1) \\ &X(\gamma_3) + R(\gamma_3) < X(\gamma_2) + R(\gamma_2) \\ &X(\gamma_3) - R(\gamma_3) < X(\gamma_2) - R(\gamma_2) \end{aligned}$$

verifying that the model does not induce any overlap between Zones I and II and between Zones III and IV. From the calculated zone relations (Eqs. (25)–(34)), one can observe an additional relationship when $\gamma_1 \leqslant \gamma \leqslant \gamma_2$ with,

$$X(\gamma_2) - R(\gamma_2) = X(\gamma_1) - R(\gamma_1) \tag{35}$$

This corresponds to a point along the X-axis where two zones overlap. But this point has no basis in physical reality as it is located in the crack ($X(\gamma) - R(\gamma) < 0 \quad \forall\gamma$). The strain field near the crack tip, at a given remote applied stress (τ_∞) is shown in Fig. 3 where the boundaries between each of the four zones and lines of constant strain in pure austenite region as well as one in the transformation zone (Zone II) are drawn.

Second, one has to verify the assumption of small-scale yielding, that the length of the plastic zone $2R(\gamma_1)$ is negligible compared to the length of the crack a. From Eq. (14), using Eqs. (16) and (26), it can be clearly seen that this assumption is valid as

$$\frac{2R(\gamma_1)}{a} = s^2 < s \ll 1$$

We have in this section fully determined the shape and the size of the austenite, the martensite and the phase transformation zone under mode III fracture. As found in mixed mode I and II (Wang et al., 2005, 2007), the size of martensitic and transformation zones increase with crack length. In addition, the radius $R(\gamma)$ is always proportional (with a factor depending on the zone) to $R(\gamma_1)$, the radius of the pure austenite zone. The distance between the center of each circle ($X(\gamma)$)and the crack tip is always smaller than the radius. Thus, the transformation zone (II) and the martensite (III + IV) completely surround the crack tip.

4. Application to Nickel–Titanium

4.1. Finite element calculations

Because the mode III fracture cannot be directly viewed experimentally to validate the theoretical model, a finite element model of a Nickel–Titanium (Nitinol) sample under mode III loading is proposed in this section. It is inspired by the work of de Morais et al. (2009).

4.1.1. Model

We consider a Nitinol sheet (Fig. 4(b)), whose dimensions are a (crack length) = 19 mm, b = 38 mm, l = 96 mm, $2h$ = 5 mm, d = 7.2 mm. When a load is applied in the four zones drawn in Fig. 4(b), de Morais et al. (2009) showed that mode III loading is dominant in the center of the sample (40 mm < y < 60 mm). Following this approach, the crack was modeled by a seam (Fig. 4(a)) using ABAQUS finite element code. By the application of increasing pressure (up to 9 GPa) on the four zones, one can observe the evolution of the stress and strain components in the vicinity of the crack tip. To prevent interpenetration of the crack surfaces, a tangential and a normal behavior ("Hard contact" in Abaqus) were defined for the two faces of the crack. As we consider an antiplane displacement, the two opposite sides of the crack develop friction, which modifies the boundary condition along the crack. A friction coefficient of 0.005 was chosen to minimize this effect. The sheet was meshed using C3D8R elements and the mesh was refined in the vicinity of the crack tip (59 μm square pattern) and where the pressure was applied (Fig. 6). We define Nitinol with an elastic–plastic stress–strain curve (Table 1) from experimental values determined by Wang et al. (2008) in their studies on mode I fracture. E_A (respectively E_M) represents Young's Modulus of Austenite (respectively of Martensite) The stress–strain relation between τ and γ is given in Fig. 5.

The plastic deformation of martensite chosen in the FEM model is slightly different from our theoretical model as it is not possible to compute the strain-hardening behavior for high value of the plastic strain. After the last values of the yield stress and plastic strain picked by the user (1.24 GPa, 0.5), a perfect plasticity model is indeed used for strains > 0.5. This difference has theoretically no effect on $R(\gamma)$ for $\gamma < \gamma_3$ but will modify $X(\gamma)$ in this interval. One other expected difference is the probable absence of strain singularity at the crack tip.

4.1.2. Results

The shape of the deformed sheet is shown in Fig. 6. The variation in colors is due to the refinement of the mesh in certain zones. There is no mechanical explanation. To observe the zone of interest, a cut in the y-plane ($y = 45$ mm) was made (Fig. 7). Here we discuss the crack tip transformation behavior at the maximum load where the small-scale yielding assumption still holds ($r/a \simeq 100$, pressure=5.5 GPa). Only the boundaries between the different zones (I–II, II–III, III–IV) are plotted. The step presented in Fig. 7 is the last increment of pressure for which the shape of the different zones boundaries is approximately a circle. As the thickness of our sample is finite (5 mm), reading directly a coherent τ_∞ in the FEM result is impossible. However, using the value of the radius of the boundary between Zones I and II and Eq. (26),

$$s = \frac{\tau_\infty}{\tau_1} = \sqrt{\frac{2R(\gamma_1)}{a}} \tag{36}$$

As the distance between two nodes is equal to 59.4 μm in Fig. 7, using Eq. (36) the experiment has to be compared with a theoretical case where s=0.19. Without calculating the shape and size of each

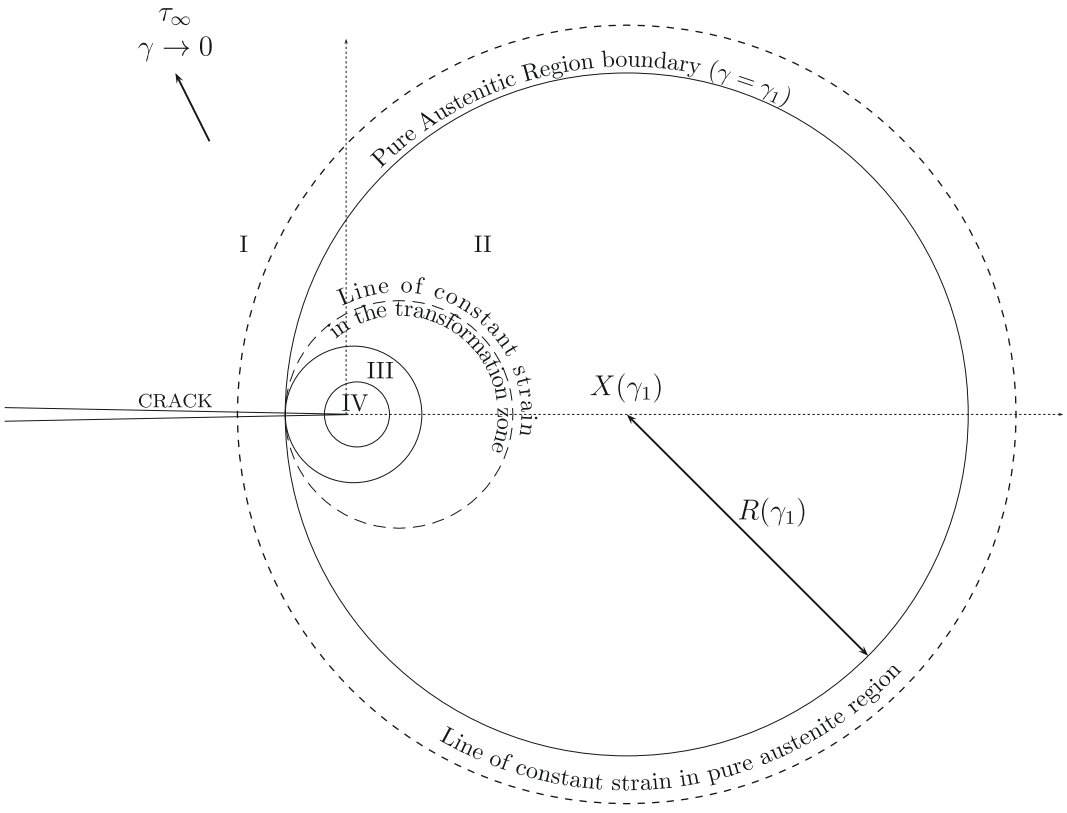

Fig. 3. Geometry of small-scale yielding near a crack for a model of SMA under mode III loading.

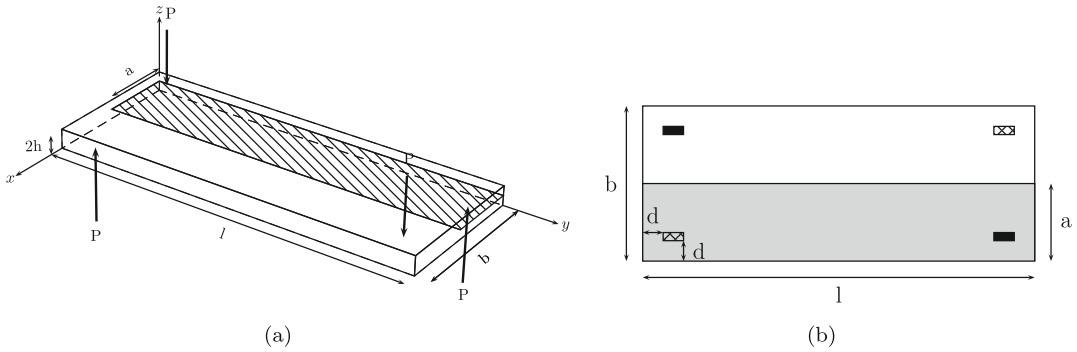

Fig. 4. (a) A top view of the Nickel–Titanium specimen used in the finite element analysis. The hatched zone in (a) represents the cracked region of the sample. (b) The zones where a uniform pressure is applied. On the upper face these zones are shown in black, hatched on the lower face. The area of one zone is equal to 1.14 mm^2.

Table 1
Mechanical behavior of NiTi used in our calculation (Wang et al., 2008).

Elastic behavior	
E_A (GPa)	$70{\cdot}10^9$
E_M (GPa)	$35{\cdot}10^9$
v	0.3
Yield stress (MPa)	Plastic strain
Plastic behavior (isotropic hardening)	
500	0
520	0.04
600	0.05
603	0.051
607	0.052
610	0.053
613	0.054
617	0.055
620	0.056
623	0.057
626	0.058
629	0.059
632	0.06
662	0.07
689	0.08
714	0.09
1240	0.5

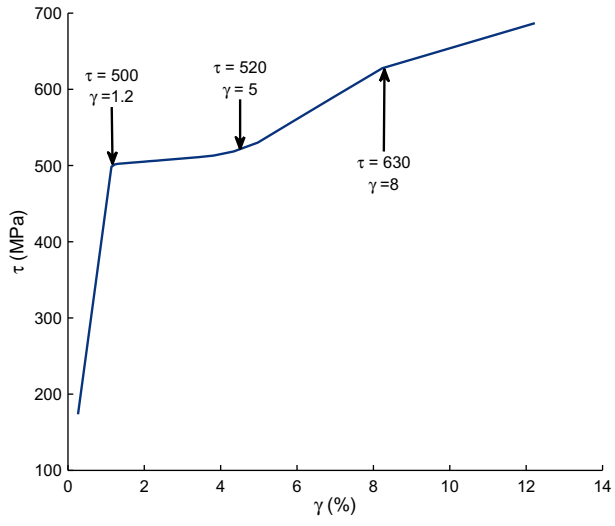

Fig. 5. stress–strain relation between γ and τ obtained in the simulation.

zone, one can reasonably suppose that our model is valid for values of $s < 0.19$. For higher values of s, the boundary between the Zones I and II is no more a circle but the zone where the stress-induced

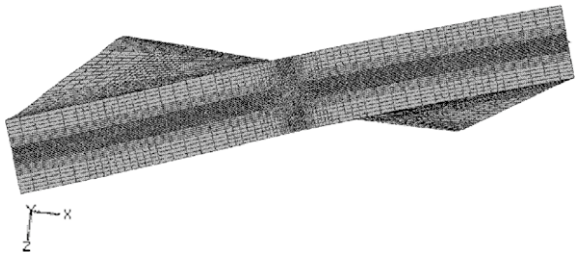

Fig. 6. NiTi sheet after the deformation.

martensite continues to get wider by keeping its shape for an applied pressure lower than 8 GPa.

4.2. Comparison with the model prediction and discussion

The stress–strain relation presented in Fig. 5 is used to determine the values for the principal stress (τ) and strain (γ) at the different boundaries for Nickel–Titanium (Table 2). The shape and size of the transformation zone and stress-induced martensite predicted by our model are then calculated for $s = 0.19$. Following the procedure outlined in Section 3, with a=19 mm and s=0.19, the theoretical distance $X(\gamma)$ ahead of the crack tip and radius $R(\gamma)$ for each zone (Table 3) are compared with the values found with the calculation. The values of simulated $X(\gamma)$ and $R(\gamma)$ are shown in Table 3. As expected, there is no strain singularity observed in our simulation. The radius of the boundary between Zones III and IV matches well, with a relative error of 7% between the theoretical and finite element model. The worst prediction concerns the boundary between the transformation zone (Zone II) and the pure stress-induced martensite zone (Zone III), where the relative error for both the radius and the center is higher than 17%. $X(\gamma)$ is always overestimated with our model by at least 22%. The main reason is that, as the zones increase in size, the outer boundaries of the body affect their shape. The absence of a strain singularity at the crack tip in the simulation may be an other cause. One other difference between the model and the calculation is that the relationship between the left extremity of the circles of constant strain in Zone II (Eq. (35)) is not respected by at most 18 μm. It does not affect the relevance of the model as it represents 8% of $R(\gamma_1)$. The major cause of this difference is due to the way we define the stress–strain relation in Abaqus/CAE. To compute the stress values in every zone, Abaqus/CAE uses the current area and not the initial area. Therefore it is difficult to have a perfect constant stress between γ_1 and γ_2 (Fig. 5).

The evolution of $X(\gamma)$ and $R(\gamma)$ with γ for $s = 0.19$ is shown in Fig. 8. As observed in various experiments of Modes I and II loading (Yi and Gao, 2000; Wang et al., 2005; Daly et al., 2007), the crack

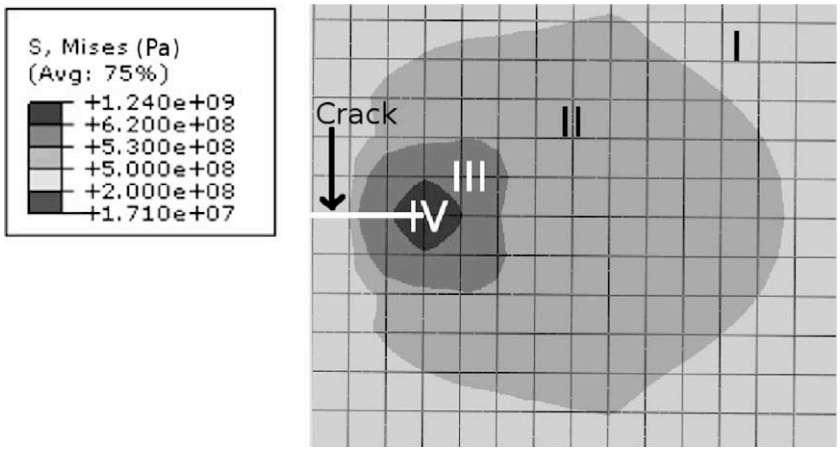

Fig. 7. Mises stress (τ) in Pa around the crack tip for y=45 mm. Applied pressure : 5.5 GPa, $s = 0.19$.

Table 2
Values for the principal stress (τ) and strain (γ) at the different boundary for Nickel–Titanium used in the theoretical model.

τ_1 (MPa)	510
τ_3 (MPa)	630
γ_1	0.012
γ_2	0.05
γ_3	0.08

Table 3
Comparison of the simulation and the theoretical values of $X(\gamma)$ and $R(\gamma)$ for Nickel–Titanium.

	Experimental value (mm)	Theoretical value (mm)	Difference (mm)	Relative error (%)
$X(\gamma_1)$	$2.30 \cdot 10^{-1}$	$2.96 \cdot 10^{-1}$	$5.9 \cdot 10^{-2}$	22
$R(\gamma_1)$	$3.42 \cdot 10^{-1}$	$3.43 \cdot 10^{-1}$	$1.4 \cdot 10^{-3}$	0.4
$X(\gamma_2)$	$2.97 \cdot 10^{-2}$	$4.40 \cdot 10^{-2}$	$1.43 \cdot 10^{-2}$	32
$R(\gamma_2)$	$10.7 \cdot 10^{-2}$	$9.15 \cdot 10^{-2}$	$1.5 \cdot 10^{-2}$	17
$X(\gamma_3)$	$1.5 \cdot 10^{-2}$	$2.05 \cdot 10^{-2}$	$5.5 \cdot 10^{-3}$	27
$R(\gamma_3)$	$4.45 \cdot 10^{-2}$	$4.16 \cdot 10^{-2}$	$4.2 \cdot 10^{-3}$	7

tip in our model (pure Mode III) is also surrounded by a zone of pure martensite ($X(\gamma) - R(\gamma)$ is always located before the crack tip). In the transformation zone ($\gamma_1 < \gamma < \gamma_2$), $X(\gamma) - R(\gamma)$ remains constant, consequence of the constant stress in this zone.

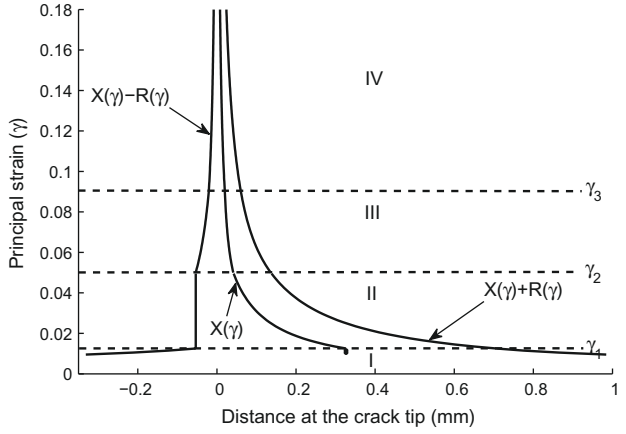

Fig. 8. Evolution of $X(\gamma)$ and $R(\gamma)$ of the circle of constant strain along the X-axis.

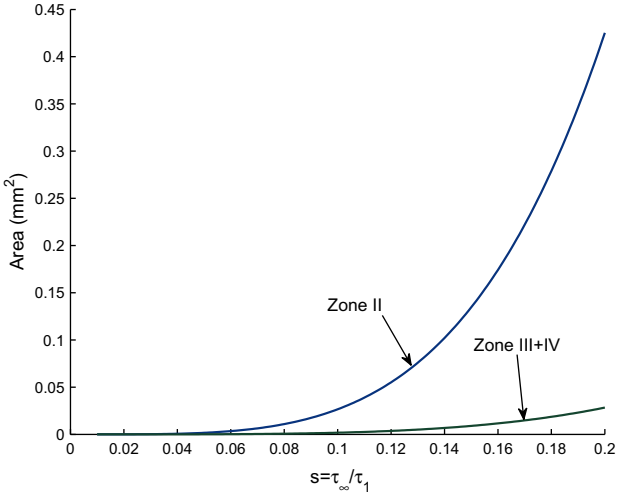

Fig. 9. Evolution of the area of the Zones II–IV with the remote applied stress.

Increasing the remotely applied stress (τ_∞), one can follow the evolution of the region of A → M phase transformation (Zone II). Fig. 9 shows a parabolic growing of its area. The area of joined Zones III and IV, corresponding to martensite under elastic loading and plastic loading respectively, stays always greatly smaller than the area encompassed by the phase transformation zone (Zone II).

5. Conclusions

This paper details a constitutive model for SMAs to determine the shape of the stress-induced A → M transformation zone in the vicinity of a crack tip under antiplane fracture. The model proposed is only valid considering a state of small-scale yielding and J2 plasticity (loading only). Due to the inherent difficulty of experimental observation of mode III fracture, the model was compared to a finite element calculation using a crack edge torsion (ECT) test. The main results from this model can be summarized as follows.

- The formation of stress-induced martensite in front of a crack tip has similarities with the formation of a plastic zone in front of a crack tip of a material which undergoes plastic deformation.
- Comparable to prior results on mode I fracture (Yi and Gao, 2000; Yi et al., 2001), the results of this analysis indicate that the crack will propagate into the stress-induced martensite under mode III fracture as well.

- As long as the assumption of small-scale yielding is valid, a zone of constant strain near the crack tip is a circle. The difference between the theoretical and computed radius $R(\gamma)$ does not exceed 10% with the exception of the boundary between the $A \rightarrow M$ transformation zone and the stress-induced martensite. The position of the zone center $X(\gamma)$ is always overestimated by at least 17%. The difference between the simulation and the model may come first from finite body effects but also from the absence of strain singularity at the crack tip in the simulation and second, from the difference in the stress–strain relation.
- The radius of the transformation zone and stress-induced martensite depend linearly on the crack length (a). The areas of these two zones are then proportional to a^2.
- The size of stress-induced martensite zone in the FEM analysis is underestimated by about 50% from the theoretical model, due largely to the difference in stress–strain relations.
- The model introduced can be easily adapted to a various range of stress–strain relations ($\tau(\gamma)$) to predict the mechanical behavior of other shape memory alloys under mode III loading.

Although the model presented has certain limitations, it captures enough of the underlying mechanics to estimate the zone where martensite is under plastic deformation to within 7% of the radius. Further extension of the model is needed in order to capture unloading and to predict the influence of multiple cycles on the shape and size of the stress-induced martensitic zone.

Acknowledgements

The authors gratefully acknowledge the support of the Ecole Polytechnique (France) and the support of the Horace H. Rackham School of Graduate Studies at the University of Michigan.

Appendix A. Supplementary data

Supplementary data associated with this article can be found, in the online version, at doi:10.1016/j.ijsolstr.2009.11.014.

References

Daly, S., Miller, A., Ravichandran, G., Bhattacharya, K., 2007. Experimental investigation of crack initiation in thin sheets of nitinol. Acta Materialia 55 (18), 6322–6330.

de Morais, A.B., Pereira, A.B., de Moura, M.F.S.F., Magalhaes, A.G., 2009. Mode iii interlaminar fracture of carbon/epoxy laminates using the edge crack torsion (ect) test. Composites Science and Technology 69 (5), 670–676.

Duerig, T., Pelton, A., Stockel, D., 1996. The utility of superelasticity in medicine. Bio-Medical Materials and Engineering 6 (4), 255–266.

Freed, Y., Banks-Sills, L., 2007. Crack growth resistance of shape memory alloys by means of a cohesive zone model. Journal of the Mechanics and Physics of Solids 55, 2157–2180.

Gollerthan, S., Young, M.L., Baruj, A., Frenzel, J., Schmahl, W.W., Eggeler, G., 2009. Fracture mechanics and microstructure in niti shape memory alloys. Acta Materialia 57 (4), 1015–1025.

Lexcellent, C., Schloemerkemper, A., 2007. Comparison of several models for the determination of the phase transformation yield surface in shape-memory alloys with experimental data. Acta Materialia 55 (9), 2995–3006.

Muskhelishvili, N., 1953. Singular Integral Equations. Noordhoff, Groningen.

Pokluda, J., Pippan, R., 2005. Can pure mode III fatigue loading contribute to crack propagation in metallic materials? Fatigue and Fracture of Engineering Materials and Structures 28 (1–2), 179–185, in: International Conference on Fatigue Crack Paths, Parma, Italy, September, 2003.

Pokluda, J., Trattnig, G., Martinschitz, C., Pippan, R., 2008. Straightforward comparison of fatigue crack growth under modes II and III. International Journal of Fatigue 30 (8), 1498–1506.

Qian, J., Fatemi, A., 1996. Mixed mode fatigue crack growth: a literature survey. Engineering Fracture Mechanics 55 (6), 969–990.

Rice, J.R., 1967. Stresses due to a sharp notch in a work-hardening elastic–plastic material loaded by longitudinal shear. Journal of Applied Mechanics 4, 287–298.

Rice, J.R., 1968. Mathematical Analysis in the Mechanics of Fracture. Academic Press.

Robertson, S.W., Mehta, A., Pelton, A.R., Ritchie, R.O., 2007. Evolution of crack-tip transformation zones in superelastic nitinol subjected to in situ fatigue: a fracture mechanics and synchrotron X-ray microdiffraction analysis. Acta Materialia 55 (18), 6198–6207.

Tschegg, E., 1982. A contribution to mode III fatigue crack propagation. Materials Science and Engineering 54 (1), 127–136.

Wang, X., Wang, Y., Baruj, A., Eggeler, G., Yue, Z., 2005. On the formation of martensite in front of cracks in pseudoelastic shape memory alloys. Materials Science and Engineering A-Structural Materials Properties Microstructure and Processing 394 (1–2), 393–398.

Wang, X., Xu, B., Yue, Z., 2008. Phase transformation behavior of pseudoelastic niti shape memory alloys under large strain. Journal of Alloys and Compounds 463, 417–422.

Wang, Y., Yue, Z., Wang, J., 2007. Experimental and numerical study of the superelastic behaviour on niti thin-walled tube under biaxial loading. Computational Materials Science 40 (2), 246–254.

Yi, S., Gao, S., 2000. Fracture toughening mechanism of shape memory alloys due to martensite transformation. International Journal of Solids and Structures 37 (38), 5315–5327.

Yi, S., Gao, S., Shen, L., 2001. Fracture toughening mechanism of shape memory alloys under mixed-mode loading due to martensite transformation. International Journal of Solids and Structures 38 (24–25), 4463–4476.